Large scale shell model calculations for the shape coexistence at $N = 40$ and $N = 50$ island of inversion*

A. N. Wu (吴阿宁)[1,2] X. P. Wang (王新鹏)[1,2] M. R. Xie (谢萌冉)[1,2] P. Y. Wang (王沛妍)[3,1] N. Chen (陈诺)[1,2]
W. Zuo (左维)[1,2†] Q. Yuan (袁琪)[1,2] J. G. Li (李健国)[1,2,4‡]

[1]State Key Laboratory of Heavy Ion Science and Technology, Institute of Modern Physics, Chinese Academy of Sciences, Lanzhou 730000, China
[2]School of Nuclear Science and Technology, University of Chinese Academy of Sciences, Beijing 100049, China
[3]Advanced Energy Science and Technology Guangdong Laboratory, 516007, Huizhou, China
[4]Southern Center for Nuclear-Science Theory (SCNT), Institute of Modern Physics, Chinese Academy of Sciences, Huizhou 516000, China

Abstract: Shape coexistence—the competition between near-degenerate spherical and deformed configurations—is a pervasive feature of neutron-rich nuclei in and around the islands of inversion. Using a large-scale shell model (LSSM) with a realistic effective interaction, we systematically compute low-lying spectra, average orbital occupations, and particle–hole (p–h) excitation probabilities to investigate candidate shape-coexistence states in even–even $N = 40$ and $N = 50$ isotones. Where data are available, our LSSM reproduces the observed systematics, including the benchmark $E(2_1^+)$ in ^{78}Ni and the characteristic shape-coexisting structure near ^{68}Ni. Along the $N = 40$ chain, $E(0_2^+)$ closely tracks $E(2_1^+)$, with a minimum at ^{64}Cr indicating maximal collectivity. Along the $N = 50$ chain, both $E(2_1^+)$ and $E(0_2^+)$ follow a parabolic evolution from ^{78}Ni to ^{70}Ca, with a common minimum at ^{74}Cr; microscopically, the 0_2^+ states are predominantly $2p$–$2h$ (with modest $3p$–$3h$/$4p$–$4h$ admixtures), while ^{74}Cr is a controlled exception, exhibiting comparable $0p$–$0h$ and $2p$–$2h$ components. When the survey is extended to neutron-rich Ti, Cr, and Fe isotopes, the LSSM captures the pronounced variation of $E(0_2^+)$, peaking at ^{62}Ti and reaching minima at $N = 50$ (^{74}Cr, ^{76}Fe), suggesting widespread shape coexistence and its evolution in these regions.

Keywords: shape coexistence, island of inversion, large-scale shell model, particle-hole excitation

DOI: 10.1088/1674-1137/aebb10 **CSTR:**

CPC Accepted

I. INTRODUCTION

The nuclear shell model (SM) has long served as a cornerstone for understanding nuclear structure [1, 2]. In the independent-particle shell-model picture, the nuclear mean field and spin-orbit splitting give rise to the conventional magic numbers 2, 8, 20, 28, 50, 82, and 126. However, this paradigm breaks down in neutron-rich nuclei with a large neutron-to-proton ratio (N/Z), where the conventional magic numbers (e.g., $N = 8$, 20 and 28) are weakened or disappear, whereas new magic numbers (e.g., $N = 14$, 16, 32 and 34) emerge [3−6]. These observations highlight the plasticity of shell structure and offer key insights into the mechanisms underlying shell evolution, many-body correlations, and nuclear collectivity.

In the traditional SM framework, nuclei with magic or semi-magic numbers are expected to possess spherical ground states. Nevertheless, low-lying deformed configurations can arise through many-particle–many-hole (mp-mh) excitations across a major shell gap (intruder configurations) in large-scale shell-model (LSSM) calculations. As protons are removed from neutron-rich magic nuclei, shell evolution can compress the spacing between single-particle orbitals straddling the magic gap, allowing intruder configurations—through enhanced quadrupole correlations—to gain more correlation energy than the normal spherical configuration. When such inversions become systematic in a region of nuclei, they delineate an "island of inversion" (IOI), such as the Ne, Na, and Mg isotopes near $N = 20$ [7, 8]. Within IOIs, strong mixing between normal and intruder configurations makes shape coexistence not exceptional but pervasive: multiple shapes (e.g., spherical, prolate, and oblate) occur at low excitation energies. Empirically, the appearance of low-lying 0^+ states in even-even nuclei constitutes a key signature of shape coexistence [9, 10]. Establishing and

Received 31 July 2026; Accepted 28 October 2026

* This work was supported by the National Key R&D Program of China under Grant Nos. 2024YFE0109800, 2024YFE0109802, and 2023YFA1606403, and by the National Natural Science Foundation of China under Grant Nos. 12405141, 12347106, 12441506, 12575124, and 12375123. The numerical calculations in this paper were performed at the Hefei Advanced Computing Center

† E-mail: zuowei@impcas.ac.cn
‡ E-mail: jianguo_li@impcas.ac.cn

©2027 Chinese Physical Society and the Institute of High Energy Physics of the Chinese Academy of Sciences and the Institute of Modern Physics of the Chinese Academy of Sciences and IOP Publishing Ltd. All rights, including for text and data mining, AI training, and similar technologies, are reserved.

quantifying shape coexistence in IOIs is therefore of broad significance: it constrains effective interactions, illuminates the mechanisms driving shell evolution, and tests many-body descriptions of emergent collectivity far from stability.

Recent experimental and theoretical studies demonstrate the merging of the inversion regions at $N = 20$ and $N = 28$ [11−13], where abundant shape coexistence phenomena are observed. The neutron-rich nucleus ^{32}Mg exhibits shape coexistence, with a spherical excited 0^+ state at 1058(2) keV and a strongly deformed ground state. Comprehensive investigations of ^{68}Ni have elucidated detailed features of shape coexistence [14−18], while revealing a nascent IOI ($N = 40$) centered on ^{64}Cr [19−23]. Simultaneously, excited spherical isomers coexisting with deformed ground states have been definitively identified in odd-odd Mn nuclei near $N = 40$ [24]. This critical evidence, combined with prior studies, experimentally establishes extensive shape coexistence across the $N = 40$ region [25, 26]. Recent experimental evidence for axial shape asymmetry and configuration coexistence in ^{74}Zn, however, suggests a potential northward extension of the $N = 40$ IOI beyond $Z = 30$ [27]. Subsequently, independent high-precision mass spectrometry using Penning traps and MR-TOF techniques, combined with LSSM calculations, has unambiguously established the coexistence of a deformed $1/2^+$ isomer (942 keV) with the spherical ground state in ^{79}Zn [28]. Furthermore, these investigations reveal compelling evidence for shared deformation mechanisms involving the doubly magic nucleus ^{78}Ni [28]. The potential appearance of shape coexistence in ^{78}Ni has also been pointed out in Ref. [29]. Combined theoretical and experimental studies near ^{78}Ni reveal emerging shape coexistence and identify a prospective $N = 50$ IOI [27, 28, 30, 31]. These established deformation mechanisms near neutron closures motivate comprehensive investigations of shape coexistence in the $N = 40$ and $N = 50$ regions [32−34].

To investigate the physical mechanisms driving shape coexistence in nuclei around the $N = 40$ and $N = 50$ regions, several theoretical approaches have been employed. For instance, both the LSSM and the Monte Carlo shell model (MCSM) have been employed to investigate shape coexistence and shell evolution in nuclei within the $N = 40$ IOI [35−37]. These approaches are complemented by state-of-the-art *ab initio* techniques such as the valence-space in-medium similarity renormalization group (VS-IMSRG) [38, 39] and coupled-cluster calculations [40], as well as by beyond-mean-field frameworks employing diverse effective interactions [33, 41]. The recently developed shell-model interaction PFSDG-U, which employs the pf shell for valence protons and the sdg shell for valence neutrons above ^{60}Ca, successfully models nuclei near $N = 50$ for proton numbers $Z = 20$ to $Z = 28$ [10]. To extend coverage beyond this domain, we perform LSSM calculations with realistic shell-model interactions. Specifically, we examine shape coexistence phenomena across the $N = 40$ and $N = 50$ IOIs, using orbital occupations and particle-hole excitation probabilities as complementary microscopic indicators of the configuration changes associated with candidate shape-coexisting states.

The article is organized as follows. First, a brief description of the realistic effective Hamiltonian is provided. This is followed by results for low-lying states in even-even nuclei with proton numbers from $Z = 20$ to $Z = 28$ and neutron numbers $N = 40$ and $N = 50$; these results are used to explore shape coexistence phenomena. Subsequently, we present neutron and proton orbital occupancies, along with particle-hole excitation configurations for the shape-coexisting 0_1^+ and 0_2^+ states. In addition, we systematically quantify the excitation energies of low-lying states and neutron occupancies across even-even neutron-rich Ti, Cr, and Fe isotopes spanning $N = 38$ to 52. Finally, we summarize the present work.

II. METHOD

Following our previous works [31, 32], we construct an effective Hamiltonian ($H_{\rm eff}$) in a valence-space configuration in which protons occupy the full pf shell, $0f_{7/2}, 1p_{3/2}, 0f_{5/2}, 1p_{1/2}$, while neutrons are active across the extended $\{1p_{1/2}, 0f_{5/2}, 0g_{9/2}, 1d_{5/2,3/2}, 2s_{1/2}\}$ orbitals. Both sets of orbitals are built above the ^{52}Ca inner core. The effective-interaction framework originates from the intrinsic Hamiltonian of an A-body system. Starting from a realistic nucleon-nucleon (NN) interaction, such as the CD-Bonn interaction [42], an effective Hamiltonian can be constructed in a truncated valence space. In our previous works [31, 32], the CD-Bonn interaction was softened using the $V_{\rm low-k}$ method with a cutoff of 2.6 fm^{-1}, and the shell-model effective interaction was derived using open-shell many-body perturbation theory [41, 43, 44], i.e., the folded-diagram $\hat{Q}$-box method, including Goldstone diagrams up to third order. The present LSSM calculations employ the effective Hamiltonian obtained in these works [31, 32]. For further technical details, see Ref. [31, 32]. Although the neutron $1p_{3/2}$ orbital is in principle relevant for maintaining SU(3) coherence, it is not included in the valence space of the present effective Hamiltonian. LSSM calculations for ^{66}Fe and ^{65}Co with the LNPS interaction [45, 46], as well as MCSM calculations for ^{66}Fe and ^{66}Co [36], show that excitations involving the neutron $1p_{3/2}$ orbital are not prominent. On this basis, we omit the neutron $1p_{3/2}$ orbital from the present valence space, although some quantitative uncertainty associated with this omission cannot be excluded.

We performed LSSM calculations using the KSHELL code [47] with the constructed shell-model effective Hamiltonian. For electric quadrupole transition strengths,

CPC Accepted

the standard effective charges $e_p = 1.5e$ and $e_n = 0.5e$ are adopted. Because the untruncated model space has a prohibitive dimensionality that exceeds the capabilities of current supercomputers, appropriate configuration truncations were necessary. We adopted suitably chosen truncations to keep the model space sufficiently large while approaching a dimension of approximately $10^{9.4}$. The largest matrix dimension encountered in our calculations was for ^{70}Cr, approximately $10^{9.54}$.

III. RESULTS

We first performed LSSM calculations for the excitation spectra of the even-even $N = 40$ isotones spanning ^{60}Ca to ^{68}Ni. The results are shown in Fig. 1, together with available experimental data [36, 48–50]. Our calculations are in agreement with the available measurements. For ^{68}Ni, the calculated 0_2^+ state lies 432 keV below the 2_1^+ state, in agreement with experimental observations and indicative of shape coexistence in ^{68}Ni. As discussed in our previous work [32], the maximum deformation occurs at ^{64}Cr, characterized by the smallest $E(2_1^+)$ values. Moreover, our calculations reveal that across the $N = 40$ isotonic chain, the $E(0_2^+)$ energies follow trends parallel to those of the $E(2_1^+)$ energies in all $N = 40$ isotones except ^{68}Ni, demonstrating rich shape coexistence in this region. In particular, ^{64}Cr exhibits the lowest 0_2^+ excitation energy among the $N = 40$ isotones. To further examine the deformation of ^{64}Cr, we calculated electric quadrupole transition strengths for ^{64}Cr. The obtained value of $B(E2; 2_1^+ \to 0_1^+) = 466.3\ e^2\text{fm}^4$ is comparable in magnitude to the experimental value of $312(79)\ e^2\text{fm}^4$ obtained from intermediate-energy Coulomb excitation [23], supporting strong quadrupole collectivity in ^{64}Cr. In addition, the much smaller calculated value of $B(E2; 0_2^+ \to 2_1^+) = 1.42\ e^2\text{fm}^4$, for which no experimental value is currently available, suggests weak mixing between the 0_2^+ state and the collective ground-state structure. These electromagnetic properties provide additional support for the coexistence of distinct low-lying structures in ^{64}Cr.

To further clarify the microscopic origin of the candidate shape-coexisting states in the $N = 40$ isotones, we calculate the orbital occupations and particle-hole excitation probabilities of the 0_1^+ and 0_2^+ states. Although orbital occupations and particle-hole excitation patterns within the LSSM do not determine deformation directly, they provide useful microscopic information on the underlying configurations associated with low-lying coexisting states. For the $N = 40$ isotones, the deviations in occupancy for the 0_1^+ and 0_2^+ states represent the differences between our LSSM average orbital occupancies and those of the conventional shell-model baseline. The results are presented in Fig. 2. Overall, the dominant proton excitations occur from the $\pi 0f_{7/2}$ orbital to the $\pi 1p_{3/2}$ and $\pi 0f_{5/2}$ orbitals, while the primary neutron excitations occur from the $\nu 0f_{5/2}$ and $\nu 1p_{1/2}$ orbitals to the $\nu 0g_{9/2}$ and $\nu 1d_{5/2}$ orbitals. In the ground state of ^{68}Ni, both proton and neutron excitations are notably suppressed, consistent with its doubly magic character. By contrast, the 0_2^+ state of ^{68}Ni displays enhanced proton and neutron excitations relative to the ground state. For ^{60}Ca, the neutron-excitation patterns in the ground state and the 0_2^+ state are similar. In ^{62}Ti, proton excitations are slightly enhanced in the 0_2^+ state compared with the ground state, while neutron excitations from the $\nu 0f_{5/2}$ orbital are reduced, with a concurrent increase in the occupation of the $\nu 1d_{5/2}$ orbital. For ^{64}Cr, both proton and neutron excitations are

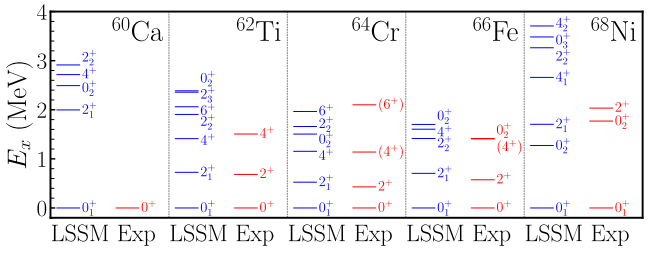


Fig. 1. (color online) The calculated energy spectrum of the even-even isotones at $N = 40$ with proton numbers ranging from $Z = 20$ (Ca) to $Z = 28$ (Ni) and the available experimental data [48–50] are shown.

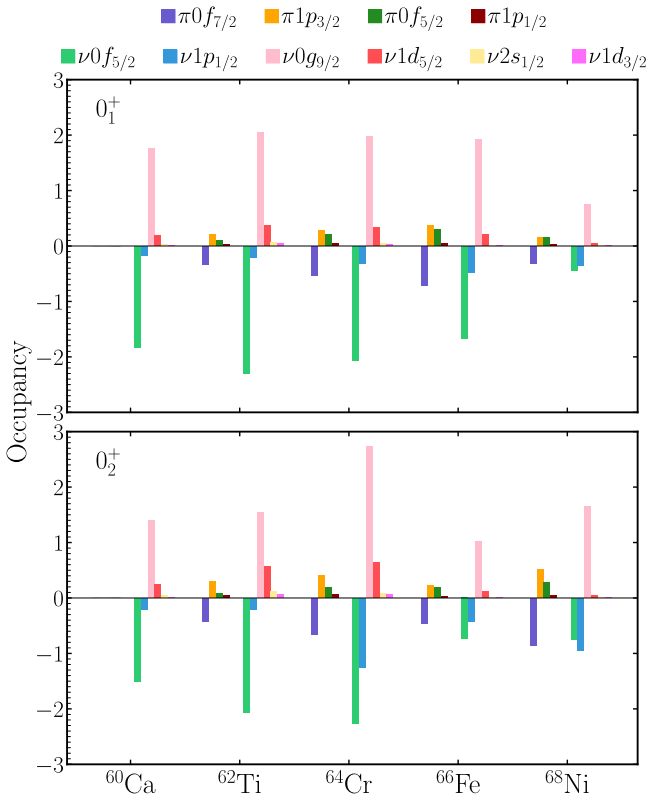


Fig. 2. (color online) The calculated deviation of proton and neutron occupancies from the expected normal filling for the 0_1^+ and 0_2^+ states in even-even isotones at $N = 40$.

CPC Accepted

strengthened in the 0_2^+ state compared with those in the ground state. In ^{66}Fe, however, both proton and neutron excitations in the 0_2^+ state are reduced relative to the ground state.

The calculated particle-hole excitation probabilities for the ground state and the 0_2^+ state are shown in Fig. 3. We adopt the conventional SM configuration associated with the $Z = 28$ shell closure and the $N = 40$ subshell closure as the $0p$-$0h$ reference. Here, the $0p$-$0h$ configuration serves only as a reference for quantifying particle-hole excitations and does not imply a robust $N = 40$ subshell closure throughout the isotonic chain. In ^{60}Ca, the particle-hole configurations are similar for the ground state and the 0_2^+ state. For ^{62}Ti, the proton configurations in the two states are nearly identical. The situation is markedly different for neutrons: the $4p$-$4h$ and $0p$-$0h$ configurations are enhanced, whereas the $2p$-$2h$ configuration is reduced in the 0_2^+ state relative to the 0_1^+ state. For ^{64}Cr, the neutron excitations in the 0_2^+ state are dominated by $2p$-$2h$ and $4p$-$4h$ configurations, with the $4p$-$4h$ component contributing nearly 80% of the total, consistent with previous LSSM calculations [33], whereas the ground state is dominated by $2p$-$2h$ configurations. The proton particle-hole excitation patterns in ^{66}Fe are analogous to those in ^{62}Ti and ^{64}Cr. For neutrons in ^{66}Fe, the ground-state excitations are more pronounced and are dominated by $2p$-$2h$ and $4p$-$4h$ configurations, with $2p$-$2h$ accounting for approximately 70%. In the 0_2^+ state, the combined contribution of $2p$-$2h$ and $4p$-$4h$ is less than 50%, and the $0p$-$0h$ configuration becomes dominant. For ^{68}Ni, both proton and neutron excitations are minimal in the ground state. In the 0_2^+ state, neutron $2p$-$2h$ configurations are dominant, with the $2p$-$2h$ component accounting for more than 70%, and proton excitations are significantly enhanced relative to the ground state; this is also consistent with previous LSSM calculations [51].

We performed analogous calculations for the $N = 50$ isotone chain to investigate shape coexistence in this region. The experimental information currently available for the $N = 50$ isotones remains limited and is essentially restricted to ^{78}Ni, which therefore serves as a crucial benchmark. Recent measurements confirm that ^{78}Ni exhibits the characteristic features of a doubly magic nucleus [29]. At the same time, a deformed rotational band has been identified in its low-lying spectrum, providing clear evidence for shape coexistence in this nucleus [29]. A variety of theoretical approaches have been applied to ^{78}Ni [10, 29], including LSSM, MCSM, coupled-cluster, and VS-IMSRG methods. These studies, together with our own LSSM calculations, generally reproduce the excitation energies of the 2_1^+ and 4_1^+ states within a reasonable range of the experimental values. In our calculations, we also obtain a high-lying 0_2^+ state in ^{78}Ni. Compared with other LSSM calculations using the PFSDG-U interaction and with MCSM results, the corresponding 0^+ state in those works appears about 700 keV lower than in our calculation. However, the calculated excitation energy of the 0_2^+ state in ^{78}Ni is not fully converged. LSSM calculations with a $4p$–$4h$ truncation yield $E(0_2^+) = 4.4$ MeV. When the truncation is extended to $5p$–$5h$, $6p$–$6h$, and $7p$–$7h$, the excitation energy of the 0_2^+ state decreases to 3.96 MeV, 3.5 MeV, and 3.3 MeV, respectively. An exponential extrapolation of these truncation-dependent results yields an estimated asymptotic excitation energy of approximately 2.8 ± 0.4 MeV, where the uncertainty reflects the dependence on the truncation range used in the extrapolation. Thus, the calculated energy of the 0_2^+ state systematically decreases as the truncation space is enlarged. However, larger truncation spaces rapidly become computationally intractable and cannot be treated within the LSSM framework. Furthermore, we have verified that the many-body configurations of the ground state of ^{78}Ni are nearly converged for the $6p$–$6h$ and $7p$–$7h$ truncations. In contrast, the calculated configurations of the 0_2^+ state still show noticeable differences among the $5p$–$5h$, $6p$–$6h$, and $7p$–$7h$ truncations, indicating that this state is not fully converged. Nevertheless, the

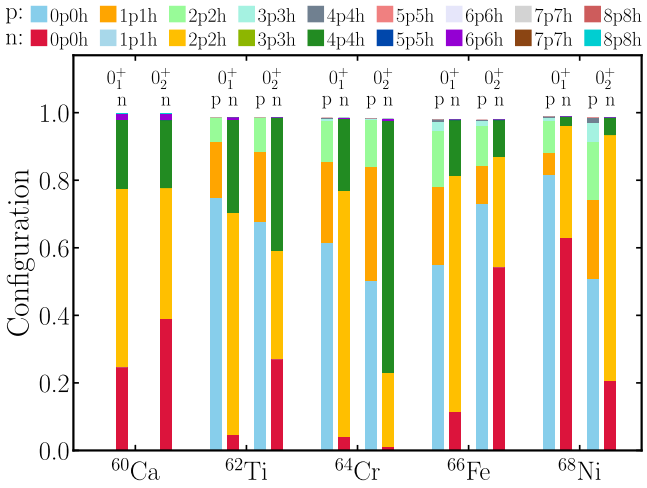


Fig. 3. (color online) Proton and neutron particle-hole excitation probabilities for the ground state and the 0_2^+ state of $N = 40$ isotones.

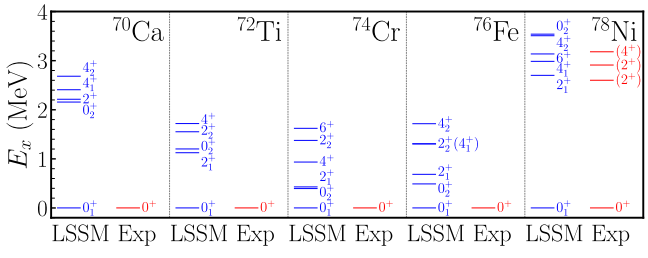


Fig. 4. (color online) The calculated energy spectrum of the even-even isotones at $N = 50$, with proton numbers ranging from $Z = 20$ (Ca) to $Z = 28$ (Ni), is shown together with available experimental data [29].

CPC Accepted

calculated wave functions consistently show that neutron $2p$–$2h$ excitations play a dominant role in the structure of the 0_2^+ state.

Similar to the $N = 40$ isotones, the trends of $E(2_1^+)$ and $E(0_2^+)$ for the $N = 50$ isotones exhibit parabolic systematics with a minimum at ^{74}Cr, where $E(2_1^+) = 427$ keV and $E(0_2^+) = 393$ keV. These trends differ markedly from those obtained in LSSM calculations with the PFSDG-U interaction [10], which predict low-lying 0_2^+ states in ^{70}Ca, ^{76}Fe, and ^{78}Ni, but rigid prolate deformation (and thus no shape coexistence) in ^{72}Ti and ^{74}Cr. For ^{74}Cr, we obtain $B(E2; 2_1^+ \to 0_1^+) = 216.0\, e^2\text{fm}^4$ and $B(E2; 0_2^+ \to 2_1^+) = 808.6\, e^2\text{fm}^4$. Experimental $B(E2)$ data are currently unavailable for this very neutron-rich nucleus. The sizable calculated transition strengths indicate pronounced quadrupole collectivity, while the strong 0_2^+–2_1^+ E2 connection suggests substantial mixing among the low-lying collective structures. Together with the low excitation energies, these results further support the shape-coexistence interpretation for ^{74}Cr and provide predictions for future experimental studies.

Deviations in orbital occupancies along the $N = 50$ isotone chain are shown in Fig. 5. Both the ground state and the 0_2^+ state exhibit complementary systematic trends. For protons, excitations increase from ^{70}Ca to ^{78}Ni, opposite to the pattern in the $N = 40$ isotone chain. In particular, the ^{78}Ni ground state shows enhanced proton excitations relative to ^{76}Fe, whereas in the $N = 40$ isotone chain the ^{68}Ni ground state exhibits reduced proton excitation compared with ^{66}Fe. Moreover, proton excitations are stronger in the ^{78}Ni ground state than in the ^{68}Ni ground state. For neutrons, the leading promotions are from $\nu 0g_{9/2}$ orbitals to the $\nu 1d_{5/2,3/2}$ and $\nu 2s_{1/2}$ orbitals. Moving from ^{78}Ni to ^{70}Ca, neutron excitations in the ground states increase, peak at ^{74}Cr, and then decrease, while those in the 0_2^+ states follow the opposite trend. Consequently, sizable differences in configuration content between the ground state and the 0_2^+ state are found for the $N = 50$ isotones (^{70}Ca, ^{72}Ti, ^{76}Fe, and ^{78}Ni), supporting the common occurrence of shape coexistence in this region.

A comparison with LSSM calculations using the PFSDG-U interaction [10] also reveals notable discrepancies in the average number of p-h excitations across the $Z = 28$ and $N = 50$ shell closures. Although the model spaces are not identical, comparing the average p-h excitations remains informative. For the 0_2^+ state of ^{78}Ni, our calculation gives about 1 proton excited across the $Z = 28$ closure and approximately 2 neutrons across the $N = 50$ closure. By contrast, LSSM calculations with the PFSDG-U interaction yield about 2.7 protons and 2.3 neutrons excited across these closures. Both the proton and neutron excitations are stronger in the LSSM calculations with the PFSDG-U interaction than in our LSSM calculations. For the ^{74}Cr and ^{72}Ti ground states, the same pattern is found

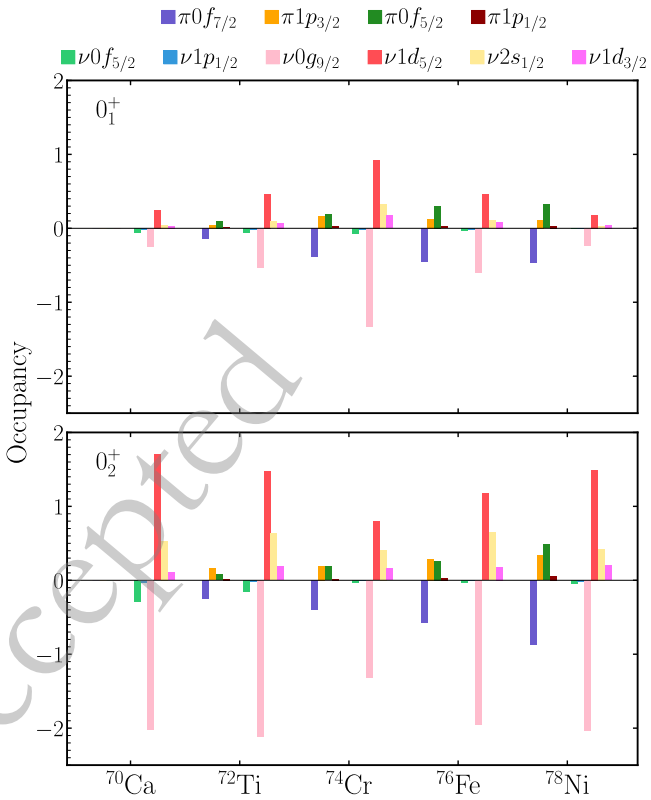


Fig. 5. (color online) The calculated deviation of proton and neutron occupancy from the expected normal filling for the 0_1^+ and 0_2^+ states in even-even $N = 50$ isotones.

for proton and neutron excitations across the closures. In particular, LSSM calculations with the PFSDG-U interaction predict stronger neutron excitation across the $N = 50$ closure, with values of 4.9 for ^{74}Cr and 4.8 for ^{72}Ti, compared with our results of 1.5 and 0.8, respectively.

For the $N = 50$ isotones, the proton and neutron particle-hole excitation probabilities for the ground state and the 0_2^+ state are calculated and shown in Fig. 6. We have taken the $Z = 28$ and $N = 50$ shell closures as reference points for studying particle-hole excitations. Along the isotone chain from ^{78}Ni to ^{70}Ca, the average $mp-mh$ excitations in the ground states increase toward ^{74}Cr, reach a maximum there, and then decrease toward ^{70}Ca. Moreover, our calculations show that the ground states of ^{74}Cr, ^{72}Ti, and ^{70}Ca are governed by neutron $0p$-$0h$ and $2p$-$2h$ configurations, whereas LSSM calculations with the PFSDG-U interaction predict dominant neutron $4p$-$4h$ configurations [10]. For the ground state of ^{76}Fe, our calculation yields about 65% neutron $0p$-$0h$ and 20% neutron $2p$-$2h$; in contrast, LSSM calculations with the PFSDG-U interaction give 21% neutron $0p$-$0h$ and 33% neutron $2p$-$2h$.

In the 0_2^+ state, the proton mp-mh excitations retain configurations similar to those of the ground state, but their strengths are noticeably enhanced in some nuclei (e.g., ^{76}Fe and ^{78}Ni). By contrast, the neutron mp-mh

CPC Accepted

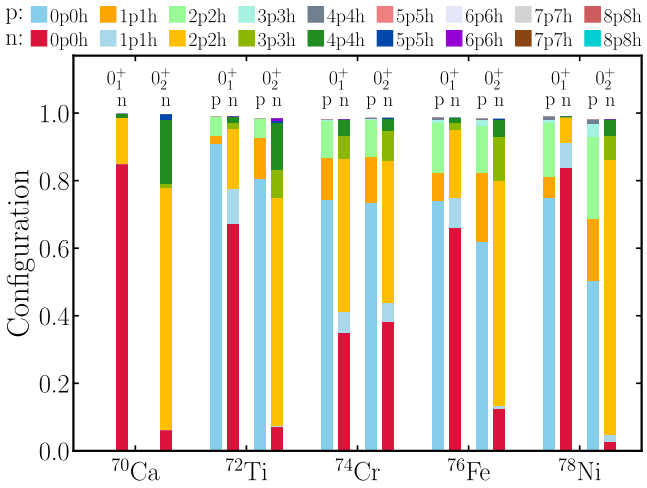


Fig. 6. (color online) Proton and neutron particle-hole excitation probabilities for the ground and 0_2^+ states of $N = 50$ isotones.

components of the 0_2^+ states differ markedly from those of the ground state for most isotones, except in ^{74}Cr, where the ground and 0_2^+ states display nearly identical configuration mixing. Overall, our calculations show that the neutron component of the 0_2^+ states is predominantly $2p$-$2h$, with non-negligible $3p$-$3h$ and $4p$-$4h$ configurations in all studied nuclei, except in ^{74}Cr, where the probabilities of $2p$-$2h$ and $0p$-$0h$ configurations are comparable. Taken together, these systematics indicate $2p$-$2h$-dominated shape coexistence in the 0_2^+ states of the $N = 50$ isotones ^{70}Ca, ^{72}Ti, ^{74}Cr, ^{76}Fe, and ^{78}Ni.

Furthermore, we performed VS-IMSRG calculations using the chiral N^{3}LO NN interaction supplemented with the N^{2}LO 3N$_{\rm lnl}$ interaction [52]. The valence space adopted in these calculations is the same as that used with the PFSDG-U interaction above the ^{60}Ca core. Our VS-IMSRG results indicate the presence of a low-lying 0_2^+ state in ^{72}Ti, ^{74}Cr, and ^{76}Fe. These results are consistent with our LSSM calculations but contrast with the LSSM results obtained using the PFSDG-U interaction.

Furthermore, we extended our LSSM to neutron-rich Ti, Cr, and Fe isotopes to investigate shell evolution, shape competition, and collective phenomena. We systematically calculated the low-lying states and neutron occupancies. The calculated excitation energies for the $0_{1,2}^+$, 2_1^+, 4_1^+, and 6_1^+ states in the neutron-rich Ti, Cr, and Fe isotopes ($N = 38$–52) are presented in Table 1, alongside available experimental data [30, 36, 48–50, 53, 55–57]. These calculations reproduce the systematics of the low-lying states in these isotopes, with the largest discrepancy relative to experimental data being approximately 460 keV for the 0_2^+ state in ^{66}Fe. In addition, for the Cr and Fe isotopes near $N = 40$, our results are in close agreement with LSSM calculations employing the LNPS interaction [30].

The energy of the 0_2^+ state exhibits significant variations with increasing neutron number across the Ti, Cr, and Fe isotopic chains. It reaches a maximum of 2386 keV in ^{62}Ti. These trends, together with additional low-lying 0_2^+ states in ^{74}Cr and ^{76}Fe at $N = 50$, indicate pervasive shape coexistence across this region.

To further investigate shape coexistence, we calculated the neutron occupancies for the ground state and the shape-coexisting 0_2^+ state along the Ti, Cr, and Fe isotopic chains. The deviations of the valence-neutron occupan-

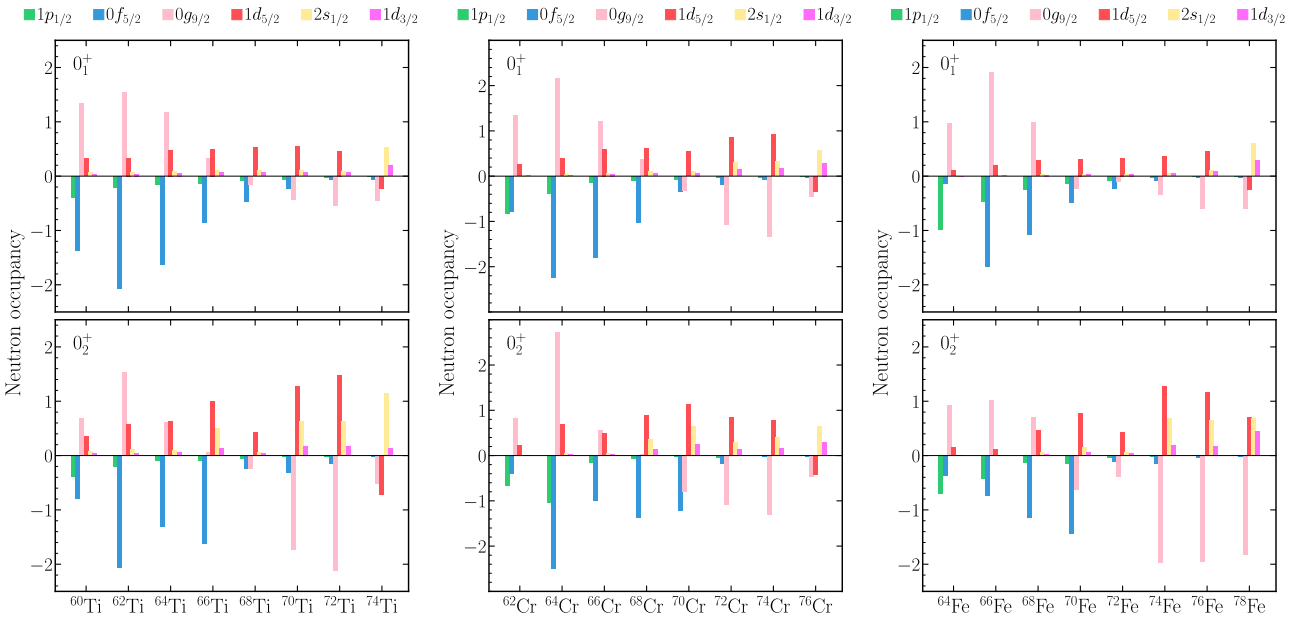


Fig. 7. (color online) Calculated deviation of neutron occupancy from the expected normal filling for the 0_1^+ and 0_2^+ states in the even-even isotopic chains of Ti, Cr, and Fe that span neutron numbers $N = 38$ to 52.

CPC Accepted

Table 1. Our LSSM calculations for the low-lying states of neutron-rich Ti, Cr, and Fe isotopes are presented together with the available experimental data.

		0_1^+	2_1^+	4_1^+	6_1^+	0_2^+	2_2^+
^{60}Ti	Theo.	0	0.775	1.496	2.193	1.842	1.623
	Expt. [53]	0	0.850	1.716			
^{62}Ti	Theo.	0	0.726	1.411	2.061	2.386	1.905
	Expt. [48]	0	0.683	1.506			
^{64}Ti	Theo.	0	0.639	1.215	1.807	1.826	1.875
^{66}Ti	Theo.	0	0.681	1.31	1.861	2.095	1.939
^{68}Ti	Theo.	0	0.664	1.281	1.872	1.924	1.623
^{70}Ti	Theo.	0	0.721	1.463	1.936	1.475	1.403
^{72}Ti	Theo.	0	1.125	1.718	2.034	1.201	1.551
^{74}Ti	Theo.	0	0.538	1.184	1.867	1.476	1.317
^{62}Cr	Theo.	0	0.59	1.24	2.019	1.325	1.423
	Expt. [54]	0	0.446	1.174	2.190	(1.379)	(1.955)
^{64}Cr	Theo.	0	0.525	1.155	1.965	1.505	1.659
	Expt. [49]	0	0.422	1.132	2.094		
^{66}Cr	Theo.	0	0.362	0.855	1.515	1.844	1.926
	Expt. [30]	0	0.386	1.069			
^{68}Cr	Theo.	0	0.489	1.064	1.831	1.483	1.957
^{70}Cr	Theo.	0	0.437	0.960	1.684	1.444	1.67
^{72}Cr	Theo.	0	0.402	0.921	1.606	0.588	0.957
^{74}Cr	Theo.	0	0.427	0.933	1.621	0.393	1.374
^{76}Cr	Theo.	0	0.471	1.129	1.840	1.257	1.476
^{64}Fe	Theo.	0	0.73	1.755	2.397	1.291	1.516
	Expt. [55, 56]	0	0.746	1.763	2.842		(1.443)
^{66}Fe	Theo.	0	0.705	1.604	2.340	1.701	1.415
	Expt. [36, 50]	0	0.573	1.407		1.414	1.881
^{68}Fe	Theo.	0	0.653	1.450	2.167	1.680	1.703
	Expt. [23, 50]	0	0.522	(1.381)			
^{70}Fe	Theo.	0	0.577	1.332	1.993	2.176	1.852
	Expt. [57]	0	0.477	1.334			
^{72}Fe	Theo.	0	0.493	1.129	1.765	2.344	2.126
	Expt. [30]	0	0.520	1.334			
^{74}Fe	Theo.	0	0.531	1.380	2.307	1.971	2.122
^{76}Fe	Theo.	0	0.684	1.305	1.93	0.49	1.305
^{78}Fe	Theo.	0	0.49	1.267	1.664	0.805	1.079

CPC Accepted

cies from a standard reference are presented in Fig. 7. Near the centers of the $N = 40$ and $N = 50$ IOIs, significant neutron excitations across these shell gaps occur in both the ground and 0_2^+ states. For nuclei midway between $N = 40$ and $N = 50$, deformation persists. Although the occupancy deviations between our LSSM and conventional SM calculations are not large, strong configuration mixing between the $\nu 0f_{5/2}$, $\nu 0g_{9/2}$, and $\nu 1d_{5/2}$ orbitals is still evident. Furthermore, the deviations in neutron occupancy are generally larger for the 0_2^+ state than for the ground state in the isotopes between $N = 40$ and $N = 50$, with ^{68}Ti as the only exception.

IV. SUMMARY

We present LSSM calculations of shape coexistence in neutron-rich nuclei around the $N = 40$ and $N = 50$ islands of inversion. The calculations reproduce the available benchmarks where data exist—most notably the first 2^+ energy of ^{78}Ni and the well-known coexistence features near ^{68}Ni. The spectroscopy identifies candidate shape-coexisting states, while the occupation and particle-hole systematics provide microscopic support for interpreting these states in terms of competing normal and intruder-like configurations. Along the $N = 40$ isotone chain (^{60}Ca–^{68}Ni), $E(0_2^+)$ tracks $E(2_1^+)$ with maximal collectivity at ^{64}Cr. Particle-hole excitation calculations corroborate these trends; for example, the 0_2^+ state of ^{64}Cr is dominated by $4p$–$4h$ (~80%), whereas the ground state is predominantly $2p$–$2h$. Along the $N = 50$ isotone chain (^{70}Ca–^{78}Ni), both $E(2_1^+)$ and $E(0_2^+)$ evolve parabolically from ^{78}Ni to ^{70}Ca, with a common minimum at ^{74}Cr. Within this chain, the 0_2^+ states are predominantly $2p$–$2h$ with modest $3p$–$3h$/$4p$–$4h$ admixtures; ^{74}Cr is a notable exception in which the $0p$–$0h$ and $2p$–$2h$ components are comparable. These results contrast quantitatively with LSSM calculations using the PFSDG-U interaction. When extended to neutron-rich Ti, Cr, and Fe isotopes ($N = 38 - 52$), our LSSM reproduces the global trends in low-lying levels, with the largest deviation of ~460 keV (for the ^{66}Fe 0_2^+ state). The 0_2^+ energy varies rapidly—peaking at ^{62}Ti and reaching minima at $N = 50$ in ^{74}Cr and ^{76}Fe.

CPC Accepted

References

[1] M. G. Mayer, Phys. Rev. **75**, 1969 (1949)

[2] O. Haxel, J. H. D. Jensen, and H. E. Suess, Phys. Rev. **75**, 1766 (1949)

[3] T. Otsuka, Physica Scripta **2013**, 014007 (2013)

[4] O. Sorlin and M.-G. Porquet, Progress in Particle and Nuclear Physics **61**, 602 (2008)

[5] W. F. Rogers, S. Garrett, A. Grovom, R. E. Anthony, A. Aulie, A. Barker, T. Baumann, J. J. Brett, J. Brown, G. Christian, P. A. DeYoung, J. E. Finck, N. Frank, A. Hamann, R. A. Haring-Kaye, J. Hinnefeld, A. R. Howe, N. T. Islam, M. D. Jones, A. N. Kuchera, J. Kwiatkowski, E. M. Lunderberg, B. Luther, D. A. Meyer, S. Mosby, A. Palmisano, R. Parkhurst, A. Peters, J. Smith, J. Snyder, A. Spyrou, S. L. Stephenson, M. Strongman, B. Sutherland, N. E. Taylor, and M. Thoennessen, Phys. Rev. C **92**, 034316 (2015)

[6] E. Becheva, Y. Blumenfeld, E. Khan, D. Beaumel, J. M. Daugas, F. Delaunay, C.-E. Demonchy, A. Drouart, M. Fallot, A. Gillibert, L. Giot, M. Grasso, N. Keeley, K. W. Kemper, D. T. Khoa, V. Lapoux, V. Lima, A. Musumarra, L. Nalpas, E. C. Pollacco, O. Roig, P. Roussel-Chomaz, J. E. Sauvestre, J. A. Scarpaci, F. Skaza, and H. S. Than, Phys. Rev. Lett. **96**, 012501 (2006)

[7] B. H. Wildenthal and W. Chung, Phys. Rev. C **22**, 2260 (1980)

[8] A. Poves and J. Retamosa, Physics Letters B **184**, 311 (1987)

[9] K. Heyde and J. L. Wood, Rev. Mod. Phys. **83**, 1467 (2011)

[10] F. Nowacki, A. Poves, E. Caurier, and B. Bounthong, Phys. Rev. Lett. **117**, 272501 (2016)

[11] P. Doornenbal, H. Scheit, S. Takeuchi, N. Aoi, K. Li, M. Matsushita, D. Steppenbeck, H. Wang, H. Baba, H. Crawford, C. R. Hoffman, R. Hughes, E. Ideguchi, N. Kobayashi, Y. Kondo, J. Lee, S. Michimasa, T. Motobayashi, H. Sakurai, M. Takechi, Y. Togano, R. Winkler, and K. Yoneda, Phys. Rev. Lett. **111**, 212502 (2013)

[12] H. Crawford, P. Fallon, A. Macchiavelli, P. Doornenbal, N. Aoi, F. Browne, C. Campbell, S. Chen, R. Clark, M. Cortés, M. Cromaz, E. Ideguchi, M. Jones, R. Kanungo, M. Maccormick, S. Momiyama, I. Murray, M. Niikura, S. Paschalis, M. Petri, H. Sakurai, M. Salathe, P. Schrock, D. Steppenbeck, S. Takeuchi, Y. Tanaka, R. Taniuchi, H. Wang, and K. Wimmer, Physical Review Letters 122 (2019), 10.1103/PhysRevLett.122.052501, cited by: 74.

[13] E. Caurier, F. Nowacki, and A. Poves, Phys. Rev. C **90**, 014302 (2014)

[14] O. Sorlin, S. Leenhardt, C. Donzaud, J. Duprat, F. Azaiez, F. Nowacki, H. Grawe, Z. Dombrádi, F. Amorini, A. Astier, D. Baiborodin, M. Belleguic, C. Borcea, C. Bourgeois, D. M. Cullen, Z. Dlouhy, E. Dragulescu, M. Górska, S. Grévy, D. Guillemaud-Mueller, G. Hagemann, B. Herskind, J. Kiener, R. Lemmon, M. Lewitowicz, S. M. Lukyanov, P. Mayet, F. de Oliveira Santos, D. Pantalica, Y.-E. Penionzhkevich, F. Pougheon, A. Poves, N. Redon, M. G. Saint-Laurent, J. A. Scarpaci, G. Sletten, M. Stanoiu, O. Tarasov, and C. Theisen, Phys. Rev. Lett. **88**, 092501 (2002)

[15] M. Hannawald, T. Kautzsch, A. Wöhr, W. B. Walters, K.-L. Kratz, V. N. Fedoseyev, V. I. Mishin, W. Böhmer, B. Pfeiffer, V. Sebastian, Y. Jading, U. Köster, J. Lettry, H. L. Ravn, and the ISOLDE Collaboration, Phys. Rev. Lett. **82**, 1391 (1999)

[16] A. Dijon, E. Clément, G. de France, G. de Angelis, G. Duchêne, J. Dudouet, S. Franchoo, A. Gadea, A. Gottardo, T. Hüyük, B. Jacquot, A. Kusoglu, D. Lebhertz, G. Lehaut, M. Martini, D. R. Napoli, F. Nowacki, S. Péru, A. Poves, F. Recchia, N. Redon, E. Sahin, C. Schmitt, M. Sferrazza, K. Sieja, O. Stezowski, J. J. Valiente-Dobón, A. Vancraeyenest, and Y. Zheng, Phys. Rev. C **85**, 031301 (2012)

[17] F. Recchia, C. J. Chiara, R. V. F. Janssens, D. Weisshaar, A. Gade, W. B. Walters, M. Albers, M. Alcorta, V. M. Bader, T. Baugher, D. Bazin, J. S. Berryman, P. F. Bertone, B. A. Brown, C. M. Campbell, M. P. Carpenter, J. Chen, H. L. Crawford, H. M. David, D. T. Doherty, C. R. Hoffman, F. G. Kondev, A. Korichi, C. Langer, N. Larson, T. Lauritsen, S. N. Liddick, E. Lunderberg, A. O. Macchiavelli, S. Noji, C. Prokop, A. M. Rogers, D. Seweryniak, S. R. Stroberg, S. Suchyta, S. Williams, K. Wimmer, and S. Zhu, Phys. Rev. C **88**, 041302 (2013)

[18] S. Suchyta, S. N. Liddick, Y. Tsunoda, T. Otsuka, M. B. Bennett, A. Chemey, M. Honma, N. Larson, C. J. Prokop, S. J. Quinn, N. Shimizu, A. Simon, A. Spyrou, V. Tripathi,

Y. Utsuno, and J. M. VonMoss, Phys. Rev. C **89**, 021301 (2014)
[19] W. Rother, A. Dewald, H. Iwasaki, S. M. Lenzi, K. Starosta, D. Bazin, T. Baugher, B. A. Brown, H. L. Crawford, C. Fransen, A. Gade, T. N. Ginter, T. Glasmacher, G. F. Grinyer, M. Hackstein, G. Ilie, J. Jolie, S. McDaniel, D. Miller, P. Petkov, T. Pissulla, A. Ratkiewicz, C. A. Ur, P. Voss, K. A. Walsh, D. Weisshaar, and K.-O. Zell, Phys. Rev. Lett. **106**, 022502 (2011)
[20] J. Ljungvall, A. Görgen, A. Obertelli, W. Korten, E. Clément, G. de France, A. Bürger, J.-P. Delaroche, A. Dewald, A. Gadea, L. Gaudefroy, M. Girod, M. Hackstein, J. Libert, D. Mengoni, F. Nowacki, T. Pissulla, A. Poves, F. Recchia, M. Rejmund, W. Rother, E. Sahin, C. Schmitt, A. Shrivastava, K. Sieja, J. J. ValienteDobón, K. O. Zell, and M. Zielińska, Phys. Rev. C **81**, 061301 (2010)
[21] A. Gade, R. V. F. Janssens, T. Baugher, D. Bazin, B. A. Brown, M. P. Carpenter, C. J. Chiara, A. N. Deacon, S. J. Freeman, G. F. Grinyer, C. R. Hoffman, B. P. Kay, F. G. Kondev, T. Lauritsen, S. McDaniel, K. Meierbachtol, A. Ratkiewicz, S. R. Stroberg, K. A. Walsh, D. Weisshaar, R. Winkler, and S. Zhu, Phys. Rev. C **81**, 051304 (2010)
[22] T. Baugher, A. Gade, R. V. F. Janssens, S. M. Lenzi, D. Bazin, B. A. Brown, M. P. Carpenter, A. N. Deacon, S. J. Freeman, T. Glasmacher, G. F. Grinyer, F. G. Kondev, S. McDaniel, A. Poves, A. Ratkiewicz, E. A. McCutchan, D. K. Sharp, I. Stefanescu, K. A. Walsh, D. Weisshaar, and S. Zhu, Phys. Rev. C **86**, 011305 (2012)
[23] H. L. Crawford, R. M. Clark, P. Fallon, A. O. Macchiavelli, T. Baugher, D. Bazin, C. W. Beausang, J. S. Berryman, D. L. Bleuel, C. M. Campbell, M. Cromaz, G. de Angelis, A. Gade, R. O. Hughes, I. Y. Lee, S. M. Lenzi, F. Nowacki, S. Paschalis, M. Petri, A. Poves, A. Ratkiewicz, T. J. Ross, E. Sahin, D. Weisshaar, K. Wimmer, and R. Winkler, Phys. Rev. Lett. **110**, 242701 (2013)
[24] S. N. Liddick, S. Suchyta, B. Abromeit, A. Ayres, A. Bey, C. R. Bingham, M. Bolla, M. P. Carpenter, L. Cartegni, C. J. Chiara, H. L. Crawford, I. G. Darby, R. Grzywacz, G. Gürdal, S. Ilyushkin, N. Larson, M. Madurga, E. A. McCutchan, D. Miller, S. Padgett, S. V. Paulauskas, J. Pereira, M. M. Rajabali, K. Rykaczewski, S. Vinnikova, W. B. Walters, and S. Zhu, Phys. Rev. C **84**, 061305 (2011)
[25] M. Sawicka, J. Daugas, H. Grawe, S. Cwiok, D. Balabanski, R. Béraud, C. Bingham, C. Borcea, M. La Commara, G. de France, G. Georgiev, M. Górska, R. Grzywacz, M. Hass, M. Hellström, Z. Janas, M. Lewitowicz, H. Mach, I. Matea, and J. Żylicz, European Physical Journal A **16**, 51 (2003)
[26] D. Pauwels, O. Ivanov, N. Bree, J. Büscher, T. E. Cocolios, J. Gentens, M. Huyse, A. Korgul, Y. Kudryavtsev, R. Raabe, M. Sawicka, I. Stefanescu, J. Van de Walle, P. Van den Bergh, P. Van Duppen, and W. B. Walters, Phys. Rev. C **78**, 041307 (2008)
[27] M. Rocchini, P. E. Garrett, M. Zielińska, S. M. Lenzi, D. D. Dao, F. Nowacki, V. Bildstein, A. D. MacLean, B. Olaizola, Z. T. Ahmed, C. Andreoiu, A. Babu, G. C. Ball, S. S. Bhattacharjee, H. Bidaman, C. Cheng, R. Coleman, I. Dillmann, A. B. Garnsworthy, S. Gillespie, C. J. Griffin, G. F. Grinyer, G. Hackman, M. Hanley, A. Illana, S. Jones, A. T. Laffoley, K. G. Leach, R. S. Lubna, J. McAfee, C. Natzke, S. Pannu, C. Paxman, C. Porzio, A. J. Radich, M. M. Rajabali, F. Sarazin, K. Schwarz, S. Shadrick, S. Sharma, J. Suh, C. E. Svensson, D. Yates, and T. Zidar, Phys. Rev. Lett. **130**, 122502 (2023)
[28] L. Nies, L. Canete, D. D. Dao, S. Giraud, A. Kankainen, D. Lunney, F. Nowacki, B. Bastin, M. Stryjczyk, P. Ascher, K. Blaum, R. B. Cakirli, T. Eronen, P. Fischer, M. Flayol, V. Girard Alcindor, A. Herlert, A. Jokinen, A. Khanam, U. Köster, D. Lange, I. D. Moore, M. Müller, M. Mougeot, D. A. Nesterenko, H. Penttilä, C. Petrone, I. Pohjalainen, A. de Roubin, V. Rubchenya, C. Schweiger, L. Schweikhard, M. Vilen, and J. Äystö, Phys. Rev. Lett. **131**, 222503 (2023)
[29] R. Taniuchi, C. Santamaria, P. Doornenbal, A. Obertelli, K. Yoneda, G. Authelet, H. Baba, D. Calvet, F. Château, A. Corsi, A. Delbart, J.-M. Gheller, A. Gillibert, J. D. Holt, T. Isobe, V. Lapoux, M. Matsushita, J. Menéndez, S. Momiyama, T. Motobayashi, M. Niikura, F. Nowacki, K. Ogata, H. Otsu, T. Otsuka, C. Péron, S. Péru, A. Peyaud, E. C. Pollacco, A. Poves, J.-Y. Roussé, H. Sakurai, A. Schwenk, Y. Shiga, J. Simonis, S. R. Stroberg, S. Takeuchi, Y. Tsunoda, T. Uesaka, H. Wang, F. Browne, L. X. Chung, Z. Dombradi, S. Franchoo, F. Giacoppo, A. Gottardo, K. Hadyńska-Klęk, Z. Korkulu, S. Koyama, Y. Kubota, J. Lee, M. Lettmann, C. Louchart, R. Lozeva, K. Matsui, T. Miyazaki, S. Nishimura, L. Olivier, S. Ota, Z. Patel, E. Şahin, C. Shand, P.-A. Söderström, I. Stefan, D. Steppenbeck, T. Sumikama, D. Suzuki, Z. Vajta, V. Werner, J. Wu, and Z. Y. Xu, Nature **569**, 53 (2019)
[30] C. Santamaria, C. Louchart, A. Obertelli, V. Werner, P. Doornenbal, F. Nowacki, G. Authelet, H. Baba, D. Calvet, F. Château, A. Corsi, A. Delbart, J.-M. Gheller, A. Gillibert, T. Isobe, V. Lapoux, M. Matsushita, S. Momiyama, T. Motobayashi, M. Niikura, H. Otsu, C. Péron, A. Peyaud, E. C. Pollacco, J.-Y. Roussé, H. Sakurai, M. Sasano, Y. Shiga, S. Takeuchi, R. Taniuchi, T. Uesaka, H. Wang, K. Yoneda, F. Browne, L. X. Chung, Z. Dombradi, S. Franchoo, F. Giacoppo, A. Gottardo, K. Hadynska-Klek, Z. Korkulu, S. Koyama, Y. Kubota, J. Lee, M. Lettmann, R. Lozeva, K. Matsui, T. Miyazaki, S. Nishimura, L. Olivier, S. Ota, Z. Patel, N. Pietralla, E. Sahin, C. Shand, P.-A. Söderström, I. Stefan, D. Steppenbeck, T. Sumikama, D. Suzuki, Z. Vajta, J. Wu, and Z. Xu, Phys. Rev. Lett. **115**, 192501 (2015)
[31] X. P. Wang, J. G. Li, and N. Chen, Phys. Rev. C **111**, 044308 (2025)
[32] J. Li, Physics Letters B **840**, 137893 (2023)
[33] S. M. Lenzi, F. Nowacki, A. Poves, and K. Sieja, Phys. Rev. C **82**, 054301 (2010)
[34] Y. Tsunoda, T. Otsuka, N. Shimizu, M. Honma, and Y. Utsuno, Phys. Rev. C **89**, 031301 (2014)
[35] N. Chen, J. G. Li, and H. H. Li, Phys. Rev. C **110**, 034316 (2024)
[36] M. Stryjczyk, Y. Tsunoda, I. G. Darby, H. De Witte, J. Diriken, D. V. Fedorov, V. N. Fedosseev, L. M. Fraile, M. Huyse, U. Köster, B. A. Marsh, T. Otsuka, D. Pauwels, L. Popescu, D. Radulov, M. D. Seliverstov, A. M. Sjödin, P. Van den Bergh, P. Van Duppen, M. Venhart, W. B. Walters, and K. Wimmer, Phys. Rev. C **98**, 064326 (2018)
[37] N. Shimizu, T. Abe, Y. Tsunoda, Y. Utsuno, T. Yoshida, T. Mizusaki, M. Honma, and T. Otsuka, Progress of Theoretical and Experimental Physics **2012**, 01A (2012)
[38] A. Tichai, K. Kapás, T. Miyagi, M. Werner, Legeza, A. Schwenk, and G. Zarand, Physics Letters B **855**, 138841 (2024)
[39] R. Silwal, C. Andreoiu, B. Ashrafkhani, J. Bergmann, T. Brunner, J. Cardona, K. Dietrich, E. Dunling, G. Gwinner, Z. Hockenbery, J. Holt, C. Izzo, A. Jacobs, A. Javaji, B. Kootte, Y. Lan, D. Lunney, E. Lykiardopoulou, T. Miyagi,

CPC Accepted

M. Mougeot, I. Mukul, T. Murböck, W. Porter, M. Reiter, J. Ringuette, J. Dilling, and A. Kwiatkowski, Physics Letters B **833**, 137288 (2022)
[40] B. Hu, Z. Sun, G. Hagen, G. Jansen, and T. Papenbrock, Phys. Lett. B **858**, 139010 (2024)
[41] L. Coraggio, A. Covello, A. Gargano, N. Itaco, T. T. S. Kuo, and R. Machleidt, Phys. Rev. C **71**, 014307 (2005)
[42] R. Machleidt, Phys. Rev. C **63**, 024001 (2001)
[43] M. Hjorth-Jensen, T. T. Kuo, and E. Osnes, Physics Reports **261**, 125 (1995)
[44] J. G. Li, B. S. Hu, Q. Wu, Y. Gao, S. J. Dai, and F. R. Xu, Phys. Rev. C **102**, 034302 (2020)
[45] B. Olaizola, L. M. Fraile, H. Mach, A. Poves, A. Aprahamian, J. A. Briz, J. Cal-González, D. Ghiţa, U. Köster, W. Kurcewicz, S. R. Lesher, D. Pauwels, E. Picado, D. Radulov, G. S. Simpson, and J. M. Udías, Journal of Physics G: Nuclear and Particle Physics **44**, 125103 (2017)
[46] B. Olaizola, L. M. Fraile, H. Mach, F. Nowacki, A. Poves, A. Aprahamian, J. A. Briz, J. Cal-González, D. Ghiţa, U. Köster, W. Kurcewicz, S. R. Lesher, D. Pauwels, E. Picado, D. Radulov, G. S. Simpson, and J. M. Udías, Phys. Rev. C **99**, 024321 (2019)
[47] N. Shimizu, T. Mizusaki, Y. Utsuno, and Y. Tsunoda, Computer Physics Communications **244**, 372 (2019)
[48] M. Cortés, W. Rodriguez, P. Doornenbal, A. Obertelli, J. Holt, S. Lenzi, J. Menéndez, F. Nowacki, K. Ogata, A. Poves, T. Rodríguez, A. Schwenk, J. Simonis, S. Stroberg, K. Yoshida, L. Achouri, H. Baba, F. Browne, D. Calvet, F. Château, S. Chen, N. Chiga, A. Corsi, A. Delbart, J.-M. Gheller, A. Giganon, A. Gillibert, C. Hilaire, T. Isobe, T. Kobayashi, Y. Kubota, V. Lapoux, H. Liu, T. Motobayashi, I. Murray, H. Otsu, V. Panin, N. Paul, H. Sakurai, M. Sasano, D. Steppenbeck, L. Stuhl, Y. Sun, Y. Togano, T. Uesaka, K. Wimmer, K. Yoneda, O. Aktas, T. Aumann, L. Chung, F. Flavigny, S. Franchoo, I. Gašparić, R.- B. Gerst, J. Gibelin, K. Hahn, D. Kim, T. Koiwai, Y. Kondo, P. Koseoglou, J. Lee, C. Lehr, B. Linh, T. Lokotko, M. MacCormick, K. Moschner, T. Nakamura, S. Park, D. Rossi, E. Sahin, D. Sohler, P.-A. Söderström, S. Takeuchi, H. Toernqvist, V. Vaquero, V. Wagner, S. Wang, V. Werner, X. Xu, H. Yamada, D. Yan, Z. Yang, M. Yasuda, and L. Zanetti, Physics Letters B **800**, 135071 (2020)
[49] A. Gade, R. V. F. Janssens, D. Bazin, P. Farris, A. M. Hill, S. M. Lenzi, J. Li, D. Little, B. Longfellow, F. Nowacki, A. Poves, D. Rhodes, J. A. Tostevin, and D. Weisshaar, Phys. Rev. C **103**, 014314 (2021)
[50] A. Gade, R. V. F. Janssens, B. A. Brown, R. G. T. Zegers, D. Bazin, P. Farris, A. M. Hill, J. Li, D. Little, B. Longfellow, F. Nowacki, D. Rhodes, and D. Weisshaar, Phys. Rev. C **104**, 024313 (2021)
[51] D. Pauwels, J. L. Wood, K. Heyde, M. Huyse, R. Julin, and P. Van Duppen, Phys. Rev. C **82**, 027304 (2010)
[52] V. Somà, P. Navrátil, F. Raimondi, C. Barbieri, and T. Duguet, Phys. Rev. C **101**, 014318 (2020)
[53] A. Gade, R. V. F. Janssens, D. Weisshaar, B. A. Brown, E. Lunderberg, M. Albers, V. M. Bader, T. Baugher, D. Bazin, J. S. Berryman, C. M. Campbell, M. P. Carpenter, C. J. Chiara, H. L. Crawford, M. Cromaz, U. Garg, C. R. Hoffman, F. G. Kondev, C. Langer, T. Lauritsen, I. Y. Lee, S. M. Lenzi, J. T. Matta, F. Nowacki, F. Recchia, K. Sieja, S. R. Stroberg, J. A. Tostevin, S. J. Williams, K. Wimmer, and S. Zhu, Phys. Rev. Lett. **112**, 112503 (2014)
[54] A. Gade, B. Longfellow, R. V. F. Janssens, D. D. Dao, F. Nowacki, J. A. Tostevin, A. D. Ayangeakaa, M. J. Basson, C. M. Campbell, M. P. Carpenter, J. ChungJung, H. L. Crawford, B. P. Crider, P. Farris, S. Gillespie, A. M. Hill, S. M. Lenzi, S. Noji, J. Pereira, C. Porzio, A. Poves, E. Rubino, and D. Weisshaar, Nature Physics **21**, 37 (2025)
[55] M. Klintefjord, J. Ljungvall, A. Görgen, S. M. Lenzi, F. L. Bello Garrote, A. Blazhev, E. Clément, G. de France, J.-P. Delaroche, P. Désesquelles, A. Dewald, D. T. Doherty, C. Fransen, A. Gengelbach, G. Georgiev, M. Girod, A. Goasduff, A. Gottardo, K. Hadyńska-Klęk, B. Jacquot, T. Konstantinopoulos, A. Korichi, A. Lemasson, J. Libert, A. LopezMartens, C. Michelagnoli, A. Navin, J. Nyberg, R. M. Pérez-Vidal, S. Roccia, E. Sahin, I. Stefan, A. E. Stuchbery, M. Zielińska, D. Barrientos, B. Birkenbach, A. Boston, L. Charles, M. Ciemala, J. Dudouet, J. Eberth, A. Gadea, V. González, L. Harkness-Brennan, H. Hess, A. Jungclaus, W. Korten, R. Menegazzo, D. Mengoni, B. Million, A. Pullia, D. Ralet, F. Recchia, P. Reiter, M. D. Salsac, E. Sanchis, O. Stezowski, C. Theisen, and J. J. Valiente Dobon, Phys. Rev. C **95**, 024312 (2017)
[56] W. W. von Seeger, P. A. DeYoung, A. Spyrou, S. Karampagia, E. F. Brown, S. Ahn, B. P. Crider, A. C. Dombos, G. W. Hitt, C. Langer, R. Lewis, S. N. Liddick, S. Lyons, Z. Meisel, F. Montes, F. Naqvi, W.-J. Ong, C. F. Persch, J. Pereira, H. Schatz, and K. Schmidt, Phys. Rev. C **109**, 044312 (2024)
[57] A. Gade, R. V. F. Janssens, J. A. Tostevin, D. Bazin, J. Belarge, P. C. Bender, S. Bottoni, M. P. Carpenter, B. Elman, S. J. Freeman, T. Lauritsen, S. M. Lenzi, B. Longfellow, E. Lunderberg, A. Poves, L. A. Riley, D. K. Sharp, D. Weisshaar, and S. Zhu, Phys. Rev. C **99**, 011301 (2019)

CPC Accepted